JACS
JOURNAL OF THE AMERICAN CHEMICAL SOCIETY
Communication
pubs.acs.org/JACS

Total Structure and Electronic Structure Analysis of Doped Thiolated Silver $[MAg_{24}(SR)_{18}]^{2-}$ (M = Pd, Pt) Clusters

Juanzhu Yan,[†] Haifeng Su,[†] Huayan Yang,[†] Sami Malola,[‡] Shuichao Lin,*[,†] Hannu Häkkinen,[‡] and Nanfeng Zheng*[,†]

[†]State Key Laboratory for Physical Chemistry of Solid Surfaces, Collaborative Innovation Center of Chemistry for Energy Materials, and Engineering Research Center for Nano-Preparation Technology of Fujian Province, College of Chemistry and Chemical Engineering, Xiamen University, Xiamen 361005, China

[‡]Departments of Physics and Chemistry, Nanoscience Center, University of Jyväskylä, FI-40014 Jyväskylä, Finland

Supporting Information

ABSTRACT: With the incorporation of Pd or Pt atoms, thiolated Ag-rich 25-metal-atom nanoclusters were successfully prepared and structurally characterized for the first time. With a composition of $[PdAg_{24}(SR)_{18}]^{2-}$ or $[PtAg_{24}(SR)_{18}]^{2-}$, the obtained 25-metal-atom nanoclusters have a metal framework structure similar to that of widely investigated $Au_{25}(SR)_{18}$. In both clusters, a M@Ag_{12} (M = Pd, Pt) core is capped by six distorted dimeric -RS-Ag-SR-Ag-SR- units. However, the silver-thiolate overlayer gives rise to a geometric chirality at variance to $Au_{25}(SR)_{18}$. The effect of doping on the electronic structure was studied through measured optical absorption spectra and ab initio analysis. This work demonstrates that modulating electronic structures by transition-metal doping is expected to provide effective means to manipulate electronic, optical, chemical, and catalytic properties of thiolated noble metal nanoclusters.

As miniatures of organic-capped metal nanoparticles, atomically precise thiolated metal nanoclusters have attracted increasing attention over the past several years.[1−4] Significant progress has been made in the synthesis and structural characterization of thiolated Au and Ag nanoclusters. The total structures of an increasing number of thiolated metal nanoclusters have been successfully characterized by X-ray crystallography,[5−18] making it possible to deeply understand the structure−properties correlation at the molecular level. Among the large number of total structures of thiolated Au nanoclusters, the presence of surface "staple" Au-thiolate units (e.g., -RS-Au-SR-, -RS-Au-SR-Au-SR-) has been commonly revealed. In comparison, the reported total structures of thiolated Ag nanoclusters (e.g., $[Ag_{44}(SR)_{30}]^{4-}$) contain surface structural motifs that are far more complicated than staple units only.[19−23] Such a structural feature makes both the molecular and electronic structures of thiolated Ag nanoclusters quite different from those of thiolated Au nanoclusters. During the past several years, much effort has been devoted to the synthesis and characterization of $Ag_{25}(SR)_{18}$[24,25] and also Ag-doped $Au_{25}(SR)_{18}$ clusters.[26,27] For instance, continuous modulation of the electronic structure of $Au_{25-n}Ag_n(SR)_{18}$ has been achieved by continuously incorporating up to 11 Ag atoms into the nanoclusters.[27] Au-rich $Au_{25-n}Ag_n(SR)_{18}$ clusters were synthesized and found to have a structure similar to that of pure $Au_{25}(SR)_{18}$.[26] Many theoretical calculations also assumed that $Ag_{25}(SR)_{18}$ would take the similar structure as well.[28,29] However, the total structure of thiolated Ag-rich 25-metal-atom nanoclusters has not been experimentally determined.

On the other hand, metal doping has been demonstrated as an effective strategy to modulate the electronic structures of thiolated Au nanoclusters, and thus their optical and possibly catalytic properties.[27,30−34] Considerable efforts have been made on doping $Au_{25}(SR)_{18}$ with Pd, Pt, Ag, Cu, Cd, and Hg.[27,30−33,35] Each $Au_{25}(SR)_{18}$ cluster consists of a centered icosahedral Au_{13} core capped by six $Au_2(SR)_3$ motifs.[6,7] Enhanced catalytic properties of the 25-atom clusters have been demonstrated by replacing the central Au atom in $Au_{25}(SR)_{18}$ with Pd or Pt.[30,31] With the incorporation of Pd or Pt atoms, we now demonstrate our success in the synthesis of two doped 25-metal-atom nanoclusters, $[MAg_{24}(SR)_{18}]^{2-}$ (M = Pd, Pt; SR = 2,4-SPhCl$_2$), and their total and electronic structures. Both clusters have a M@Ag_{12} (M = Pd, Pt) core capped by six heavily distorted staple -RS-Ag-SR- units. For the first time, such distorted staple motifs are revealed on thiolated metal nanoclusters. Unexpectedly, the presence of surface distorted staple motifs gives rise to a surface chirality on $[MAg_{24}(SR)_{18}]^{2-}$ (M = Pd, Pt). The UV−vis absorption features of $[PdAg_{24}(SR)_{18}]^{2-}$ are systematically red-shifted as compared to those of $[PtAg_{24}(SR)_{18}]^{2-}$.

To incorporate Pd into thiolated Ag nanoclusters, a modified synthesis process of $[Ag_{44}(SR)_{30}]^{4-}$ was adopted.[19] $PdCl_2$ was introduced together with $AgNO_3$ as the metal precursors in the synthesis (see Supporting Information for details). In a typical synthesis of Pd-doped Ag nanoclusters, $AgNO_3$ was dissolved in methanol. Dichloromethane and $PdCl_2$ were then added to the solution to form a mixture. The mixture was cooled to 0 °C in an ice bath, and 2,4-dichlorobenzenethiol and tetraphenylphosphonium bromide (PPh_4Br) were then added. After 20 min, $NaBH_4$ aqueous solution and triethylamine were added quickly to the above mixture under vigorous stirring. The reaction was aged for 12 h at 0 °C. The aqueous phase was then removed. The mixture in organic phase was washed several times with water for various characterizations. As clearly illustrated in Figure 1a, the obtained crude product exhibited a UV−vis absorption spectrum with two

Received: July 10, 2015
Published: September 9, 2015

DOI: 10.1021/jacs.5b07186
J. Am. Chem. Soc. 2015, 137, 11880−11883

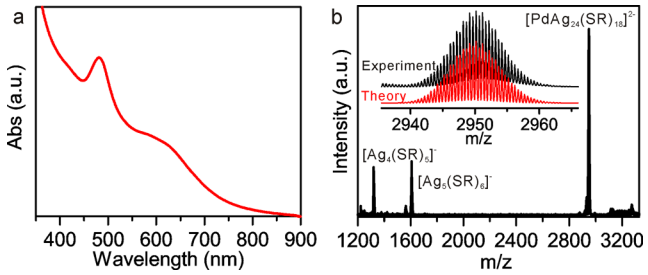

Figure 1. UV–vis (a) and ESI-MS (b) spectra of the as-prepared crude product of Pd-doped thiolated Ag nanoclusters. Inset in (b) shows both experimental and simulated high-resolution MS spectra of the major MS peak.

well-defined molecule-like optical transitions centered with the two distinct peaks at 483 and 628 nm. The absorption spectrum was different from those of $[Ag_{44}(SR)_{30}]^{4-}$, indicating the formation of new thiolated Ag nanoclusters.

To chemically identify its composition, the obtained nanocluster was characterized by electrospray ionization time-of-flight mass spectrometry (ESI-TOF-MS). As shown in Figure 1b, the as-prepared Pd-doped thiolated Ag nanoclusters displayed three main peaks centered at m/z of 2950.21, 1606.12, 1320.25. The careful analysis on the high-resolution mass data revealed that the strongest peak at m/z = 2950.21 belonged to $[PdAg_{24}(2,4\text{-}SPhCl_2)_{18}]^{2-}$ whose isotopic pattern perfectly matched the simulation. The other two major peaks were assigned to $[Ag_5(2,4\text{-}SPhCl_2)_6]^-$ and $[Ag_4(2,4\text{-}SPhCl_2)_5]^-$, respectively (Figure S1), which could be fragments of the cluster or polymeric -Ag-SR- structures formed during the synthesis. Both UV–vis and ESI-MS data clearly indicated the presence of high-purity $[PdAg_{24}(SR)_{18}]^{2-}$ in the crude products.

The high purity of $[PdAg_{24}(SR)_{18}]^{2-}$ in the crude products encouraged us to crystallize them into single crystals. High-quality dark-red single crystals (Figure S2) containing $[PdAg_{24}(SR)_{18}]^{2-}$ were obtained by slowly diffusing hexane into the CH_2Cl_2 solution of the doped nanoclusters at 0 °C. X-ray single crystal analysis did confirm the chemical formula of the $[PdAg_{24}(SR)_{18}]^{2-}$ nanocluster and its −2 charge. In the single crystals, $[PdAg_{24}(SR)_{18}]^{2-}$ nanoclusters are co-crystallized with the counter cations, PPh_4^+, in a molar ratio of 1:2, into space group of $P2_1/c$ (Figure S3). The thermogravimetric analysis (TGA) of the crystal sample of the cluster was also carried out to verify its composition. A total weight loss of ∼58.5 wt % (Figure S4) was in perfect agreement with the organic component of $(PPh_4)_2[PdAg_{24}(2,4\text{-}SPhCl_2)_{18}]$ (organic, 59.0 wt %; metal, 41.0 wt %).

Structurally, the $[PdAg_{24}(SR)_{18}]^{2-}$ nanocluster can be described as a centered icosahedral Pd@Ag_{12} core stabilized by six distorted dimeric staple -RS-Ag-SR-Ag-SR- motifs (Figure 2), having an overall framework structure similar to that of $Au_{25}(SR)_{18}$.[6,7] Several studies have attempted to prepare thiolated Ag-containing 25-metal-atom nanoclusters by doping $Au_{25}(SR)_{18}$ with Ag atoms and succeeded in replacing up to 11 Au atoms with Ag. This work represents the first successful structure determination of thiolated M_{25} clusters consisting of Ag atoms as the major framework metal atoms.

Although $[PdAg_{24}(SR)_{18}]^{2-}$ has a similar metal framework as that of $Au_{25}(SR)_{18}$, they show small variation in their detailed core structure, but significant variation in their detailed surface structures. In $[PdAg_{24}(SR)_{18}]^{2-}$, the Pd–Ag distances between Pd and the Ag_{12} cage are averaged at 2.748 Å, and the Ag–Ag bond

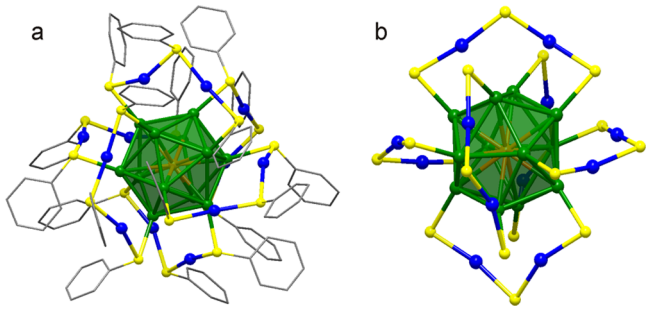

Figure 2. Structure of the $[PdAg_{24}(SR)_{18}]^{2-}$ cluster revealed by X-ray single crystal analysis. (a) The overall structure of the cluster. (b) The capping structure of six-distorted dimeric -RS-Ag-SR-Ag-SR- surface staple motifs on the centered icosahedral Pd@Ag_{12} core. Color legend: green and blue spheres, Ag; orange sphere, Pd; yellow sphere, S; gray sphere, C. All hydrogen and chlorine atoms are omitted for clarity.

lengths in Ag_{12} cage in $[PdAg_{24}(2,4\text{-}SPhCl_2)_{18}]^{2-}$ nanoclusters range from 2.970 to 2.810 Å. With the incorporation of Pd at the center, the metal–metal bonds in the icosahedral core have an averaged distance of 2.849 Å, slightly shorter than those (averaged at 2.87) in $Au_{25}(SR)_{18}$.[6,7] On the surface of $Au_{25}(SR)_{18}$, each of the six Au atoms is linearly bound by two SR with ∠S–Au–S ranging from 171.8 to 174.1°. In comparison with the fairly linear coordination of surface Au atom on $Au_{25}(SR)_{18}$, the ∠S–Ag–S bond angles of the 12 surface Ag atoms on $[PdAg_{24}(SR)_{18}]^{2-}$ range from 144.8 to 173.7°, having a much bigger variation. As a result, the six dimeric -RS-Ag-SR-Ag-SR- surface staple motifs are not planar any more (Figure 3A and S5). In each staple unit, at least one of two terminal SR^- groups is heavily deviated from the plane defined by the middle three atoms, -Ag-SR-Ag-.

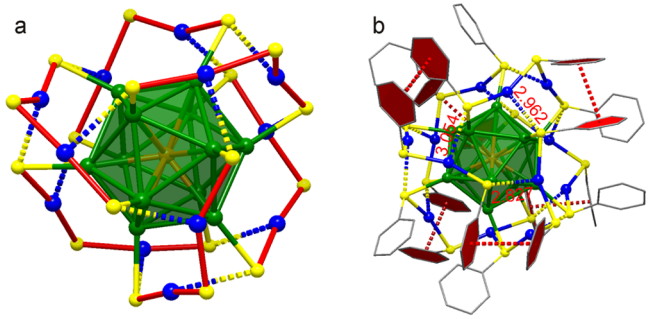

Figure 3. Structures showing the important surface structure features of $[PdAg_{24}(SR)_{18}]^{2-}$. (a) The structure highlighting the interactions within the six-distorted dimeric surface staple motifs (colored in red sticks). Dashed sticks are used to illustrate the Ag···S interactions between neighboring motifs. (b) The structure showing six π stacked ligand pairs on the surface. The stacked ligand pairs are highlighted as red hexagons connected by dash red lines.

It should be noted that the presence of distorted dimeric -RS-Ag-SR-Ag-SR- staple motifs on the surface of $[PdAg_{24}(SR)_{18}]^{2-}$ largely alters the interactions between neighboring staple units. The two terminal SR^- groups in each dimeric staple motif interact with two Ag atoms from its two different adjacent staple motifs. Totally, there are therefore 12 pairs of Ag···S interactions on the cluster's surface. The Ag···S distances range 2.777 from 3.330 Å with an average of 3.006 Å (Figure 3a and S6). In comparison, the similar Au···S contacts in $Au_{25}(SR)_{18}$ are all longer than 3.72 Å.[6,7] With 12 pairs of Ag···S interactions, $[PdAg_{24}(SR)_{18}]^{2-}$ can be alternatively structurally described as an icosahedral Pd@Ag_{12}

DOI: 10.1021/jacs.5b07186
J. Am. Chem. Soc. 2015, 137, 11880–11883

core protected by four triangular surface $[(AgSR)_3(SR)_{3/2}]$ units. We consider the incorporation of Pd is the key to the successful synthesis of $[PdAg_{24}(SR)_{18}]^{2-}$ having a similar metal framework structure but distorted surface structure to that of $Au_{25}(SR)_{18}$. The synthesis in the absence of Pd precursor led to the formation of $[Ag_{44}(SR)_{30}]^{2-}$ as the main product (Figure S7).

Another important surface structural feature of $[PdAg_{24}(SR)_{18}]^{2-}$ is the presence of strong $\pi\cdots\pi$ interactions between six pairs of benzene rings in thiolate ligands(Figure 3b). Together with the Ag···S interactions discussed above, such $\pi\cdots\pi$ interactions help to lock the arrangement of surface ligands and create surface chirality. In the crystals of $[PdAg_{24}(SR)_{18}]^{2-}$, two enantiomers with the four surface $[(AgSR)_3(SR)_{3/2}]$ units arranged in two different orientations (Figure S8). Unfortunately, the two enantiomers were 1:1 ratio to give no circular dichroism (CD) signals.

An analogous attempt was also made to synthesize Pt-doped Ag nanoclusters. When K_2PtCl_4 was used to replace $PdCl_2$ as the dopant precursor, the obtained nanoclusters showed a major mass peak centered at m/z of 2994.24 (Figure 4). Detailed analysis on

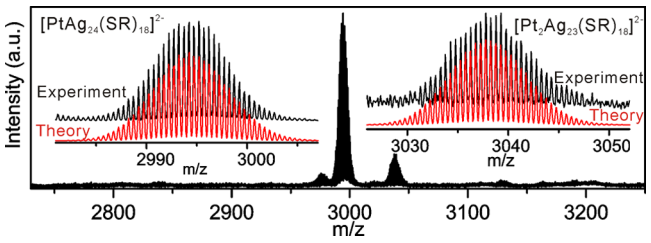

Figure 4. ESI-MS spectra of the as-prepared crude product of Pt-doped thiolated Ag nanoclusters. The insets are the corresponding high-resolution spectra. Insets show both experimental and simulated high-resolution MS spectra of the two major MS peaks.

its high-resolution mass data suggested that the Pt-doped Ag nanoclusters had a composition of $[PtAg_{24}(SR)_{18}]^{2-}$. The presence of small amount of $[Pt_2Ag_{24}(SR)_{18}]^{2-}$ was also revealed in the ESI-MS spectrum of the as-prepared Pt-doped nanoclusters. The single crystal analysis confirmed that the obtained $[PtAg_{24}(SR)_{18}]^{2-}$ indeed have a similar structure to that of $[PdAg_{24}(SR)_{18}]^{2-}$ (Figure S9). The much heavier electron density at the center clearly suggested that the central atom should be Pt. The second Pt atom in $[Pt_2Ag_{23}(SR)_{18}]^{2-}$ should be located at any site of the 12 positions at the icosahedral shell. Crystallographically, the small amount of $[Pt_2Ag_{23}(SR)_{18}]^{2-}$ would not be expected to make detectable contribution to the electron densities at the 12 atom positions of the icosahedral shell. It should also be noted that the peak for $[Pt_2Ag_{23}(SR)_{18}]^{2-}$ observed in the ESI-MS spectra (Figure S10) of dissolved crystals was much weaker than that of the crude product. In some cases, the peak was even undetectable. These results suggested that $[Pt_2Ag_{23}(SR)_{18}]^{2-}$ should have relatively poor stability and thus would not survive much during the crystallization process.

The doping of Pd and Pt alters the electronic structure of the thiolated Ag nanoclusters. As compared to Ag that contains one free valence s-electron ($d^{10}s^1$ configuration), Pd has a closed d-shell but no s-electrons ($d^{10}s^0$), while Pt has both d and s shells open (d^9s^1). It is then of interest to study how these transition-metal dopants contribute to the overall electronic structure of the $[MAg_{24}(SR)_{18}]^{2-}$. Our analysis of the frontier orbitals of $[MAg_{24}(SR)_{18}]^{2-}$ (M = Pd, Pt) clusters show unambiguously that the clusters have overall 8 free valence electrons, namely, the 3-fold degenerate HOMO state is a superatom 1P, and the lowest empty superatom 1D states are split in 2-fold LUMO and 3-fold LUMO+1 manifolds just as in the previous case of $[Au_{25}(SR)_{18}]^{-}$.[7,36] Thus, the clusters obey the widely applied superatom rule (Figure S11).[37] It is important to realize that the 24 − 18 + 2 = 8 electron count for $[MAg_{24}(SR)_{18}]^{2-}$ (M = Pd, Pt) comes from the 24 Ag(s) electrons, minus 18 electrons withdrawn by the thiolates, plus two extra electrons from the overall negative charge, implying that both Pd and Pt act as zerovalent dopants in these clusters. Pt thus acts as a closed d-shell $d^{10}s^0$ element as dopant, not d^9s^1 as in the free atom. The relative positions of the Ag and Pd/Pt d-electrons are revealed in Figure S12: the upper edge of the Ag(4d)-band is at about −3.7 eV, while the Pd(4d)/Pt(5d) dopant band is located at around −2.5 eV.

Figure 5 shows that both $[PdAg_{24}(SR)_{18}]^{2-}$ and $[Pt_xAg_{24-x}(SR)_{18}]^{2-}$ (x = 1, 2) exhibit broad multiband optical

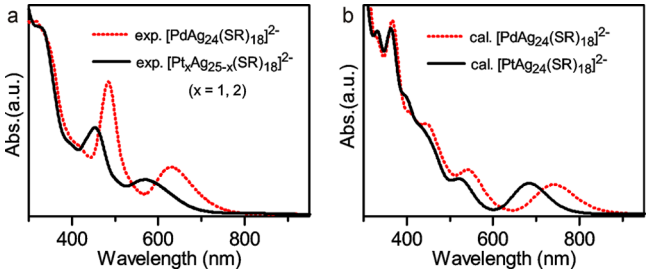

Figure 5. Experimental (a) and computed (b) UV−vis spectra of $[PdAg_{24}(SR)_{18}]^{2-}$ and $[PtAg_{24}(SR)_{18}]^{2-}$ nanoclusters. In the theoretical spectra, the individual optical transitions have been folded into a smooth curve by using a Gaussian width of 0.1 eV.

absorptions in the UV−vis region. $[PdAg_{24}(SR)_{18}]^{2-}$ displays two major absorption peaks centered at 483 and 628 nm. In comparison, the two major absorption peaks of $[Pt_xAg_{24-x}(SR)_{18}]^{2-}$ (x = 1, 2) were blue-shifted to 453 and 564 nm, respectively. Such a blue shift in the optical absorption is consistent with the previous studies on Pd/Pt-doped Au_{25} nanoclusters. The calculated spectra are systematically red-shifted compared to the experiment, but they reproduce very well the relative shifts between $[PdAg_{24}(SR)_{18}]^{2-}$ and $[PtAg_{24}(SR)_{18}]^{2-}$ in the two lowest-energy peaks (Table S1). The lowest-energy peaks for $[PdAg_{24}(SR)_{18}]^{2-}$ are systematically red-shifted compared to the $[PtAg_{24}(SR)_{18}]^{2-}$. This correlates with the smaller calculated HOMO−LUMO gap for $[PdAg_{24}(SR)_{18}]^{2-}$ (1.45 eV) vs $[PtAg_{24}(SR)_{18}]^{2-}$ (1.61 eV).

The calculations also strongly indicated that Pd must be at the center of $[PdAg_{24}(SR)_{18}]^{2-}$, although X-ray crystallography cannot distinguish well between Pd and Ag. The total energies of three different structures of $[PdAg_{24}(SR)_{18}]^{2-}$ with the Pd atom located at the icosahedral center, the icosahedral shell, and the surface metal−ligand shell were also calculated for the comparison of their stabilities. The relative stabilities were calculated to be 0, + 0.65, and +0.87 eV, respectively, for the three structures with Pd moving from the center to the metal−ligand shell. Moreover, the calculated optical spectra on the structure with Pd doped at the icosahedral center matched the best with the measured data as compared to the other two structures (Figure S13). Moreover, a hypothetical all-silver $[Ag_{25}(SR)_{18}]^{-}$ cluster with the same structure as $[PdAg_{24}(SR)_{18}]^{2-}$ except replacing the central Pd atom by Ag was found to have a calculated optical spectrum (Figure S14) very similar to that of $[PdAg_{24}(SR)_{18}]^{2-}$ and also previously reported spectra of $[Ag_{25}(SR)_{18}]^{-}$.[24,25] These

DOI: 10.1021/jacs.5b07186
J. Am. Chem. Soc. 2015, 137, 11880−11883

results clearly suggested that all-silver $[Ag_{25}(SR)_{18}]^-$ should have a similar total structure as $[PdAg_{24}(SR)_{18}]^{2-}$ reported in this work.

As observed directly from the crystal structure analysis of $[MAg_{24}(SR)_{18}]^{2-}$, the silver-thiolate overlayer imposes geometric chirality, and both enantiomers are present 1:1 in the crystal unit cell. Figure S15 shows the calculated CD spectra for one enantiomer of $[PdAg_{24}(SR)_{18}]^{2-}$, $[PtAg_{24}(SR)_{18}]^{2-}$, and the hypothetical $[Ag_{25}(SR)_{18}]^-$ discussed above. All the clusters have also very similar CD spectra, where the signals in the range of 450−900 nm are red-shifted in $[PdAg_{24}(SR)_{18}]^{2-}$ compared to $[PtAg_{24}(SR)_{18}]^{2-}$. Our calculation serves here as a prediction for experimental CD spectra in case that the enantiomeric separation will be achieved in the future experiments.[38]

To summarize, by introducing Pd or Pt, thiolated Ag-rich 25-metal-atom nanoclusters with a composition of $[MAg_{24}(SR)_{18}]^{2-}$ (M = Pd or Pt) have been successfully synthesized and structurally identified by X-ray diffraction. Both clusters can structurally described as a $M@Ag_{12}$ (M = Pd, Pt) core capped by six distorted dimeric -RS-Ag-SR-Ag-SR- staple units, having a metal framework structure similar to that of the widely studied $[Au_{25}(SR)_{18}]^-$ cluster. Ag-rich thiolated 25-metal-atom nanoclusters have been long pursued but not structurally characterized. This work has clearly demonstrated the importance of metal doping in tuning electronic structures of metal nanoclusters. Modulating electronic structures by transition-metal doping is expected to provide effective means to manipulate electronic, optical, chemical, and catalytic properties of thiolated noble metal nanoclusters.

■ ASSOCIATED CONTENT

Supporting Information

The Supporting Information is available free of charge on the ACS Publications website at DOI: 10.1021/jacs.5b07186.

Experimental details, detailed crystallographic structure and data, computational details, analysis of the cluster electronic structure, TGA, and more mass spectra (PDF)
Crystallographic data (CIF)
Crystallographic data (CIF)

■ AUTHOR INFORMATION

Corresponding Authors

*nfzheng@xmu.edu.cn
*sclin@xmu.edu.cn

Notes

The authors declare no competing financial interest.

■ ACKNOWLEDGMENTS

We thank the MOST of China (2011CB932403, 2015CB932303) and the NSFC of China (21420102001, 21131005, 21390390, 21227001, 21333008) for financial support. The work in University of Jyväskylä was supported by the Academy of Finland (266492). The computations were made at the CSC computing center in Espoo, Finland.

■ REFERENCES

(1) Jin, R. *Nanoscale* **2015**, *7*, 1549.
(2) Qian, H. F.; Zhu, M. Z.; Wu, Z. K.; Jin, R. C. *Acc. Chem. Res.* **2012**, *45*, 1470.
(3) Häkkinen, H. *Nat. Chem.* **2012**, *4*, 443.
(4) Tsukuda, T. *Bull. Chem. Soc. Jpn.* **2012**, *85*, 151.
(5) Jadzinsky, P. D.; Calero, G.; Ackerson, C. J.; Bushnell, D. A.; Kornberg, R. D. *Science* **2007**, *318*, 430.
(6) Heaven, M. W.; Dass, A.; White, P. S.; Holt, K. M.; Murray, R. W. *J. Am. Chem. Soc.* **2008**, *130*, 3754.
(7) Zhu, M.; Aikens, C. M.; Hollander, F. J.; Schatz, G. C.; Jin, R. *J. Am. Chem. Soc.* **2008**, *130*, 5883.
(8) Qian, H. F.; Eckenhoff, W. T.; Zhu, Y.; Pintauer, T.; Jin, R. C. *J. Am. Chem. Soc.* **2010**, *132*, 8280.
(9) Das, A.; Li, T.; Nobusada, K.; Zeng, C.; Rosi, N. L.; Jin, R. *J. Am. Chem. Soc.* **2013**, *135*, 18264.
(10) Dass, A.; Theivendran, S.; Nimmala, P. R.; Kumara, C.; Jupally, V. R.; Fortunelli, A.; Sementa, L.; Barcaro, G.; Zuo, X.; Noll, B. C. *J. Am. Chem. Soc.* **2015**, *137*, 4610.
(11) Zeng, C.; Chen, Y.; Kirschbaum, K.; Appavoo, K.; Sfeir, M. Y.; Jin, R. *Sci. Adv.* **2015**, *1*, e1500045.
(12) Zeng, C.; Liu, C.; Chen, Y.; Rosi, N. L.; Jin, R. *J. Am. Chem. Soc.* **2014**, *136*, 11922.
(13) Das, A.; Li, T.; Li, G.; Nobusada, K.; Zeng, C.; Rosi, N. L.; Jin, R. *Nanoscale* **2014**, *6*, 6458.
(14) Crasto, D.; Malola, S.; Brosofsky, G.; Dass, A.; Häkkinen, H. *J. Am. Chem. Soc.* **2014**, *136*, 5000.
(15) Zeng, C. J.; Li, T.; Das, A.; Rosi, N. L.; Jin, R. C. *J. Am. Chem. Soc.* **2013**, *135*, 10011.
(16) Zeng, C.; Qian, H.; Li, T.; Li, G.; Rosi, N. L.; Yoon, B.; Barnett, R. N.; Whetten, R. L.; Landman, U.; Jin, R. *Angew. Chem., Int. Ed.* **2012**, *51*, 13114.
(17) Das, A.; Li, T.; Nobusada, K.; Zeng, Q.; Rosi, N. L.; Jin, R. *J. Am. Chem. Soc.* **2012**, *134*, 20286.
(18) Yang, H. Y.; Wang, Y.; Edwards, A. J.; Yan, J. Z.; Zheng, N. F. *Chem. Commun.* **2014**, *50*, 14325.
(19) Yang, H. Y.; Wang, Y.; Huang, H. Q.; Gell, L.; Lehtovaara, L.; Malola, S.; Häkkinen, H.; Zheng, N. F. *Nat. Commun.* **2013**, *4*, 2422.
(20) Desireddy, A.; Conn, B. E.; Guo, J.; Yoon, B.; Barnett, R. N.; Monahan, B. M.; Kirschbaum, K.; Griffith, W. P.; Whetten, R. L.; Landman, U.; Bigioni, T. P. *Nature* **2013**, *501*, 399.
(21) Yang, H. Y.; Lei, J.; Wu, B. H.; Wang, Y.; Zhou, M.; Xia, A. D.; Zheng, L. S.; Zheng, N. F. *Chem. Commun.* **2013**, *49*, 300.
(22) Yang, H. Y.; Wang, Y.; Zheng, N. F. *Nanoscale* **2013**, *5*, 2674.
(23) Zhang, X.; Yang, H. Y.; Zhao, X. J.; Wang, Y.; Zheng, N. F. *Chin. Chem. Lett.* **2014**, *25*, 839.
(24) Cathcart, N.; Mistry, P.; Makra, C.; Pietrobon, B.; Coombs, N.; Jelokhani-Niaraki, M.; Kitaev, V. *Langmuir* **2009**, *25*, 5840.
(25) Chakraborty, I.; Udayabhaskararao, T.; Pradeep, T. *J. Hazard. Mater.* **2012**, *211−212*, 396.
(26) Kumara, C.; Aikens, C. M.; Dass, A. *J. Phys. Chem. Lett.* **2014**, *5*, 461.
(27) Negishi, Y.; Iwai, T.; Ide, M. *Chem. Commun.* **2010**, *46*, 4713.
(28) Bakr, O. M.; Amendola, V.; Aikens, C. M.; Wenseleers, W.; Li, R.; Dal, N. L.; Schatz, G. C.; Stellacci, F. *Angew. Chem., Int. Ed.* **2009**, *48*, 5921.
(29) Aikens, C. M. *J. Phys. Chem. C* **2008**, *112*, 19797.
(30) Xie, S.; Tsunoyama, H.; Kurashige, W.; Negishi, Y.; Tsukuda, T. *ACS Catal.* **2012**, *2*, 1519.
(31) Qian, H.; Jiang, D.-e.; Li, G.; Gayathri, C.; Das, A.; Gil, R. R.; Jin, R. *J. Am. Chem. Soc.* **2012**, *134*, 16159.
(32) Christensen, S. L.; MacDonald, M. A.; Chatt, A.; Zhang, P.; Qian, H.; Jin, R. *J. Phys. Chem. C* **2012**, *116*, 26932.
(33) Negishi, Y.; Munakata, K.; Ohgake, W.; Nobusada, K. *J. Phys. Chem. Lett.* **2012**, *3*, 2209.
(34) Jin, R.; Nobusada, K. *Nano Res.* **2014**, *7*, 285.
(35) Wang, S.; Song, Y.; Jin, S.; Liu, X.; Zhang, J.; Pei, Y.; Meng, X.; Chen, M.; Li, P.; Zhu, M. *J. Am. Chem. Soc.* **2015**, *137*, 4018.
(36) Akola, J.; Walter, M.; Whetten, R. L.; Häkkinen, H.; Grönbeck, H. *J. Am. Chem. Soc.* **2008**, *130*, 3756.
(37) Walter, M.; Akola, J.; Lopez-Acevedo, O.; Jadzinsky, P. D.; Calero, G.; Ackerson, C. J.; Whetten, R. L.; Gronbeck, H.; Häkkinen, H. *Proc. Natl. Acad. Sci. U. S. A.* **2008**, *105*, 9157.
(38) Lopez-Acevedo, O.; Tsunoyama, H.; Tsukuda, T.; Häkkinen, H.; Aikens, C. M. *J. Am. Chem. Soc.* **2010**, *132*, 8210.

DOI: 10.1021/jacs.5b07186
J. Am. Chem. Soc. 2015, 137, 11880−11883